Untangling the Mechanics and Topology in the Frictional Response of Long Overhand Elastic Knots

M. K. Jawed,[1] P. Dieleman,[2] B. Audoly,[3,*] and P. M. Reis[1,2,†]
[1]Department of Mechanical Engineering, Massachusetts Institute of Technology, Cambridge, Massachusetts 02139, USA
[2]Department of Civil and Environmental Engineering, Massachusetts Institute of Technology, Cambridge, Massachusetts 02139, USA
[3]Sorbonne Universités, UPMC Univ Paris 06, CNRS, UMR 7190 Institut Jean Le Rond d'Alembert, F-75005 Paris, France
(Received 23 April 2015; revised manuscript received 7 August 2015; published 11 September 2015)

We combine experiments and theory to study the mechanics of overhand knots in slender elastic rods under tension. The equilibrium shape of the knot is governed by an interplay between topology, friction, and bending. We use precision model experiments to quantify the dependence of the mechanical response of the knot as a function of the geometry of the self-contacting region, and for different topologies as measured by their crossing number. An analytical model based on the nonlinear theory of thin elastic rods is then developed to describe how the physical and topological parameters of the knot set the tensile force required for equilibrium. Excellent agreement is found between theory and experiments for overhand knots over a wide range of crossing numbers.

DOI: 10.1103/PhysRevLett.115.118302 PACS numbers: 46.25.-y, 02.10.Kn, 46.70.Hg

Shoelaces are commonly tied using the *reef* knot, which comprises two trefoil knots: the first is left handed and the other right handed. Mistakenly tying two consecutive left-handed trefoil knots leads to the mechanically inferior *granny* knot [1], whose lower performance illustrates the important interplay between topology and mechanics. From polymer chains [2] to the shipping industry, knots are ubiquitous across length scales [3]. Whereas they can appear spontaneously [4] and are sometimes regarded as a nuisance (e.g., in hair and during knitting), knots as fasteners of filamentary structures have applications in biophysics [5], surgery [6,7], fishing [8], sailing [9], and climbing [10]. Frictional knots have also been added to fibers for increased toughness [11].

Even if the quantitative study of knots has remained primarily in the realm of pure mathematics [12], there have been empirical attempts to characterize their mechanical properties according to strength or robustness [13,14]. However, these metrics rely strongly on material-specific properties and are therefore of limited applicability across different systems and length scales [3]. Recent studies have addressed the mechanics of knots from a more fundamental perspective [15,16]. For example, existing theories on flexible strings (with zero bending stiffness) [17,18] treat friction using the capstan equation [19]. Finite element simulations of knots have also been performed in instances where bending cannot be neglected [20] and friction has been treated perturbatively for trefoil knots tied in elastic rods [21,22]. Still, predictively understanding the mechanics of knots remains a challenging endeavor, even for the simplest types of elastic knots, due to the complex coupling of the various physical ingredients at play.

Here, we perform a systematic investigation of elastic knots under tension and explore how their mechanical response is influenced by topology. We perform precision model experiments and rationalize the observed behavior through an analysis based on Kirchhoff's geometrically nonlinear model for slender elastic rods. Our theory takes into account regions of self-contact, where friction dominates. Focus is given to open *overhand* knots [Figs. 1(a)–1(d)]. These knots comprise a braid with arc

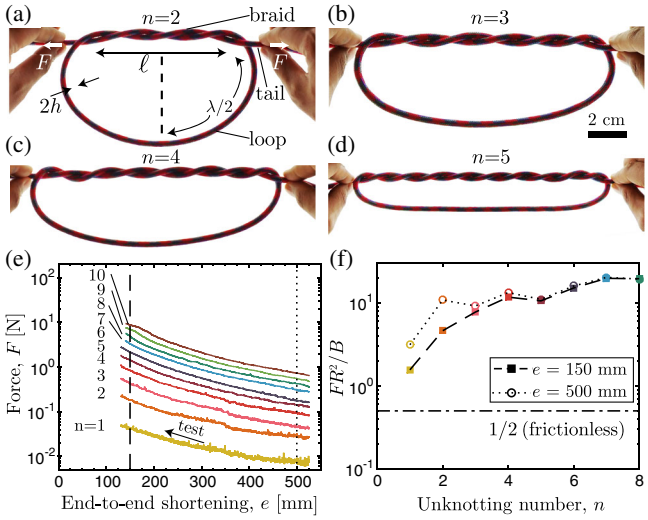

FIG. 1 (color online). (a)–(d) Photographs of overhand knots with different unknotting numbers n. A piece of rope (5 mm diam) is used here for illustration purposes, although all the experiments described in the text used Nitonol rods (see Fig. S2 in Ref. [23]). (e) Traction force vs end-to-end shortening for overhand knots in Nitonol rods with radius $h = 0.127$ mm and $1 \leq n \leq 10$. (f) Normalized traction force FR^2/B as a function of unknotting number n at $e = \{150, 500\}$ mm [dashed and dotted lines in (e)]. The horizontal solid line at $1/2$ corresponds to the frictionless case.

length ℓ, a loop with arc length λ, and two tails onto which a tensile load is applied. The topology of the braid is quantified by the *unknotting number* $n = (\chi - 1)/2$ (number of times the knot must be passed through itself to untie it), where χ is the *crossing number* (number of apparent crossing nodes). In Fig. 1(e), we plot the traction force F as a function of the end-to-end shortening, e ($e = 0$ corresponds to a straight configuration, without a knot) for a variety of knots in the range $1 \leq n \leq 10$. We find that F depends nonlinearly on e and varies significantly with n. We shall provide an analytical solution for the relation between the knot topology (defined by n) and the braid geometry. We then extend our analysis to identify the underlying physical ingredients and predictively capture the experimental mechanical response.

Our experiments consisted of tying overhand knots on Nitinol rods (662 mm long) of circular cross section with radius $h = 0.127$ mm density $\rho = 6450$ kg/m^3 and Young's modulus, $E = 67.50 \pm 0.25$ GPa. One extremity of the rod was clamped. The other end was attached to the load cell of a universal testing machine (Instron) and displaced slowly to tighten the initially loose knot from $e_{\text{start}} = 531$ mm, at a rate of $(-\dot{e}) = 1$ mm/s (such that inertial effects are negligible). During the process we recorded the resulting tensile force F, required to maintain the equilibrium configuration; there are more details in the Supplemental Material [23]. In Fig. 1(e), we present a series of $F(e)$ curves for knots with unknotting numbers in the range $1 \leq n \leq 10$, and find that the mechanical response is dramatically affected by n. During these tests, we also make use of digital imaging to record the braid geometry and the shape of the loop.

In prior work, the mechanics of knots has been analyzed using a string model with the assumptions of finite friction but neglecting bending [17], using the capstan equation [19]. These theories for "ideal knots" on a perfectly flexible filament under tension predict the end-to-end shortening to be $e = hf(n)$, where the function f depends only on the topology of the knot (e.g., see Ref. [18]). By contrast, in our experiments, a string model is clearly inappropriate since the bending stiffness $B = E\pi h^4/4$ plays a key role in setting the shape of the loop, such that $e \gg h$. More subtly, we shall show that the bending stiffness is also important in the braid, where both strands adopt an approximately helical configuration of radius h. The curvature of each strand scales as $\sim hk^2$, where k is its wave number, and equilibrium under a tension F requires a normal force per unit length $\sim Fhk^2$ (arising from contact with the other braid) that is correctly captured by the string model. However, the bending rigidity neglected in the string model leads to an additional contribution to the normal force per unit length that can be shown to scale as $\sim Bhk^4$, as our analysis below will confirm. If the string model were to be applicable, the first contribution would have to dominate and the ratio $F/(Bk^2)$ would be large. In Fig. 2(d), we plot this ratio for our experiments and find that it is always lower than 1, thereby showing that the stiffness of the filament must be accounted for [the rationale for $2\pi nhk$ on the x axis of Fig. 2(d) is provided below].

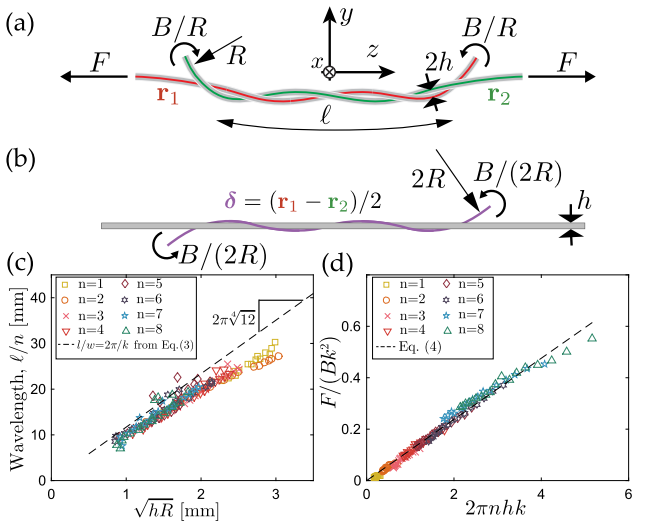

FIG. 2 (color online). (a)–(b) Geometry of the braid. (a) The two centerlines $\mathbf{r}_1$ and $\mathbf{r}_2$ effectively wrapped around a flexible cylinder with diameter $2h$. (b) The difference braid effectively winds around a rigid cylinder, with both ends subjected to a moment $Q \sim B/(2R)$. (c) Wavelength of the braid, $\ell/n = 2\pi/k$, as a function of $\sqrt{hR}$. (d) Traction force F normalized by Bk^2 as a function of $2\pi hkn$.

Knots in stiff filaments have been previously analyzed [21] but only in the perturbative limit of $\mu \to 0$ (and $B \neq 0$). This approach is also not applicable for our experiments as the following dimensional analysis demonstrates. Each strand in the braid is subject to three forces: (i) the traction force F due to the tensile load exerted on the tails, (ii) the pulling force $B/(2R^2)$ applied by the elastic loop of radius R [2,21], and (iii) the friction force resulting from self-contact in the braid. In the absence of friction, the first two forces balance each other and $FR^2/B = 1/2$. In Fig. 1(f), we revisit the raw data for $F(e)$ and plot the dimensionless force FR^2/B. For $n = 1$, $FR^2/B \approx 2$, the same order of magnitude as the value of $1/2$ for the frictionless case [horizontal solid line in Fig. 1(f)]. In this particular case of trefoil knots, the weak friction assumption used by Ref. [21] is acceptable. However, $FR^2/B \gg 1/2$ for all other higher-order knots ($n \geq 2$, which from now on we shall refer to as *long* knots), indicating that friction is important and must be taken into account, in full. Motivated by these findings, and in contrast with prior work, we seek to develop a theory to describe long knots that incorporates both the bending rigidity B and the strong effect of friction μ.

A schematic diagram of the configuration of the braid region for $n > 1$ is shown in Fig. 2(a). We shall use an elastic curve model where twisting forces are ignored and assume that the aspect ratio between the cross-sectional

radius of the rod h and the radius of curvature at the exit from the braid towards the loop R is small, i.e., $\epsilon = \sqrt{h/R} \ll 1$. This results in a separation of length scales $h \ll (\ell/n) \ll R$, such that the theory of slender rods is applicable [23]. The braid can then be modeled by two *linear* beams in mutual contact whose centerlines are represented by $\mathbf{r}_1(z)$ and $\mathbf{r}_2(z)$, with the z axis aligned along the traction force.

We now consider the *difference problem* by focusing on the relative position of the two strands: $\boldsymbol{\delta}(z) = [\mathbf{r}_1(z) - \mathbf{r}_2(z)]/2 + z\mathbf{e}_z$, shown schematically in Fig. 2(b). In the limit of $\epsilon \to 0$, $\boldsymbol{\delta}(z)$ can be determined through asymptotic analysis of the braid by mapping the problem to the winding of a linear beam around a rigid cylinder [21]. The nonpenetration condition implies $\delta_x^2 + \delta_y^2 \geq h^2$, which effectively represents a cylindrical obstacle with radius h. Given the invariance of $\boldsymbol{\delta}(z)$ by a rotation about the y axis with angle π, we further simplify the analysis by only considering the half-braid ($z > 0$). Far away from the braid, the curvatures of the strands should match those in the tail and in the loop, $(\mathbf{r}_1'', \mathbf{r}_2'') \to (\mathbf{e}_y/R, \mathbf{0})$ for $z \gg \ell/2$, where the primes refer to differentiation with respect to s. This yields $\boldsymbol{\delta}''(z) \to \mathbf{e}_y/(2R)$, meaning that in the difference problem a remote bending moment $-B/(2R)\mathbf{e}_x$ needs to be applied.

The total energy of the braid can now be obtained by doubling the energy of the half-braid:

$$E_{\text{braid}} = 2\left(\frac{B}{2}\int_0^L |\boldsymbol{\delta}''|^2 dz - \frac{B}{2R}\boldsymbol{\delta}'(L)\cdot\mathbf{e}_y\right). \quad (1)$$

This linear beam model can be derived from the nonlinear Kirchhoff rod model in the limit $h \ll (\ell/n) \ll R$ (see Ref. [22]): the first term is an elastic beam energy and the second term arises from the moment that enforces the asymptotic curvature $1/(2R)$ far from the braid. The integration in Eq. (1) is done over a segment of the rod enclosing one half-braid, i.e., $L > \ell/2$, but the particular choice of L does not affect the solution $\boldsymbol{\delta}$. The configuration of the braid can then be determined by minimizing Eq. (1) with respect to $\boldsymbol{\delta}$, subject to the nonpenetration constraint $\delta_x^2 + \delta_y^2 \geq h^2$, as well as the conditions that capture the topology of the knot: $\varphi(0) = -n\pi$ and $0 \leq \varphi(L) \leq \pi$, where $\varphi(z)$ is the polar angle of the projection of $\boldsymbol{\delta}(z)$ in the perpendicular plane (Oxy).

The above minimization problem with inequality constraints has previously been solved numerically for trefoil and cinquefoil knots ($n = 1$ and $n = 2$) [21]. Our goal is to now obtain an analytical solution that is applicable for long knots. For $n \gg 1$, we can ignore the inner layers present near the end points of the braid $z = \pm\ell/2$. In this limit, we consider an approximation $\boldsymbol{\delta}(z)$ obtained by patching a helix of radius h that winds $n/2$ turns around the $z > 0$ semiaxis (half-braid), together with a parabola in the (Oyz) plane of the loop with curvature $1/(2R)$, as prescribed by the end moment

$$\boldsymbol{\delta}(z) = \begin{cases} (h\cos\varphi, h\sin\varphi, z) & \text{if } 0 \leq z \leq \frac{\ell}{2} \\ \left(h, \left(z - \frac{\ell}{2}\right)\left(kh + \frac{z-\frac{\ell}{2}}{4R}\right), z\right) & \text{if } \frac{\ell}{2} \leq z \leq L, \end{cases} \quad (2)$$

where $\varphi = -n\pi + kz$. The helical wave number $k = d\varphi/dz$ is a free parameter that is still to be determined, from which the braid length can eventually be computed as $\ell = 2n\pi/k$, implying $\varphi(\ell/2) = 0$. Note that this approximation is kinematically admissible; it satisfies the nonpenetration condition, it has the correct unknotting number, and both the position $\boldsymbol{\delta}(z)$ and the tangent $\boldsymbol{\delta}'(z)$ are continuous at $z = \ell/2$. The 2D assumption in this solution is in agreement with the nearly planar loop observed in the experiments [23].

Inserting the approximation of Eq. (2) into Eq. (1) and eliminating ℓ in favor of k, we find an energy of the braid $E_{\text{braid}} = -(BL/4R^2) + (\epsilon^3/h)Bn\pi\bar{E}(\bar{k})$, where $\bar{E} = \bar{k}^3 + (1/4\bar{k})$ and $\bar{k} = kh/\epsilon = k\sqrt{hR}$. Terms of order $1/n$ have been neglected in $\bar{E}$. The optimal wave number k is found by solving $\partial_k E_{\text{braid}} = 0$, which yields $\partial_{\bar{k}}\bar{E} = 0$ and, consequently, $\bar{k} = 1/\sqrt[4]{12}$, or equivalently in physical variables,

$$k = (\sqrt{12}(hR))^{-1/2}. \quad (3)$$

In Fig. 2(c), we compare the predicted wavelength $2\pi/k = \ell/n = 2\pi\sqrt[4]{12}\sqrt{hR}$ against our experimental data and find good agreement between the two, thereby validating the analysis thus far. The total braid length then reads $\ell = 2n\pi/k = 2w_c\sqrt{2hR}$, where $w_c(n) = \pi n/(\sqrt{2}\bar{k}) = \sqrt[4]{3\pi n}$ in the large-n limit under consideration. Extrapolating this formula to trefoil and cinquefoil knots, even if not valid *a priori* since the assumption of $n \gg 1$ is violated, yields $w_c(n = 1) = 4.13$ and $w_c(n = 2) = 8.27$. These values are within 20% and 10%, respectively, of the exact values of $w_c^*(n = 1) = 3.51$ and $w_c^*(n = 2) = 7.60$, calculated by a numerical solution that accounts for the boundary layers [21]. This supports the appropriateness of the helical approximation in Eq. (2), even for small n.

Having characterized the geometry of the braid, we proceed by evaluating the *scalar* contact force P integrated along the entire region of contact. Following a variational approach, we consider a virtual increase, from h to $h + dh$, of the radius of the effective cylinder around which the braid winds. The work done by the contact force is Pdh. Since P appears to be the force conjugate to the cylinder radius h, its equilibrium value can be calculated as $P = \partial_h E_{\text{braid}} = \bar{E}(\bar{k})Bn\pi/\sqrt{4hR^3}$, with $\bar{E}(\bar{k}) = 4/12^{3/4} = 4\bar{k}^3$ at equilibrium. This yields the contact pressure $P = 2n\pi Bhk^3$ for large n, which can be interpreted as the product of the braid length $\ell = 2n\pi/k$ with the lineic density of contact force Bhk^4 that is required to deform an elastic curve into a helix with radius h and pitch $2\pi/k$.

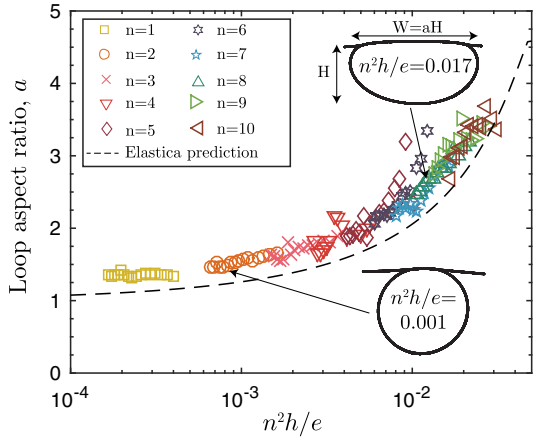

FIG. 3 (color online). Aspect ratio of the loop $a = W/H$ as a function of n^2h/e. The dashed line (theory) was calculated by solving the nonlinear planar Elastica problem of the loop [23].

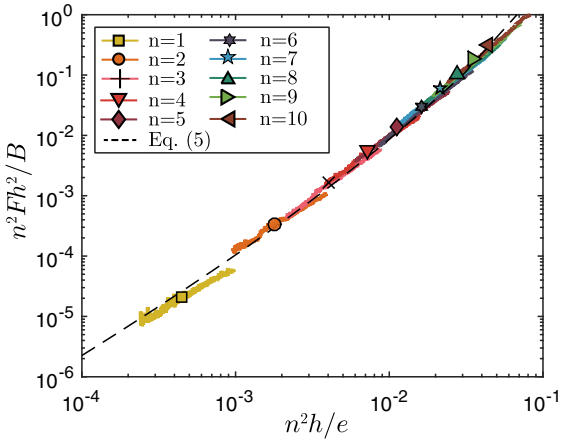

FIG. 4 (color online). When plotted using the dimensionless variables suggested by the theory, the experimental traction curves [from Fig. 1(e)] for knots in the range $1 \le n \le 10$ collapse onto a master curve predicted by Eq. (5) (dashed line).

Using Coulomb's law of friction, the integrated contact force P can now be connected to the traction force F measured in the experiments. We further assume that the braid remains nearly straight, and that the internal force in the loop, $\sim B/R^2$, is negligible compared to the traction force F applied by the operator on the tails [supported by our experimental data, since $FR^2/B \gtrsim 20$ for $n \ge 3$; see Fig. 1(f)]. Under these assumptions, the main contribution to the traction force F arises primarily from friction. As such, $F = \mu P$, which after combining with the expression for P derived above, yields

$$\frac{F}{Bk^2} = \mu 2\pi nhk. \tag{4}$$

In Fig. 2(d), we test this prediction against experiments by plotting $F/(Bk^2)$ versus $2\pi nhk$. All the data for knots with different values of n collapse onto a linear master curve. The slope is a measure of the dynamic friction coefficient, $\mu = 0.119 \pm 0.001$, obtained by fitting.

Thus far, we have found two equations, Eqs. (3) and (4), for the three unknowns (k, F, R) in terms of the parameters (n, B, h, μ). To close the system, we derive a third equation by solving the nonlinear planar Elastica problem for the shape of the loop and obtain its arc length λ (and, consequently, also the end-to-end shortening, $e = \lambda + \ell$) as a function of both ℓ and R. Owing to scale invariance, this dependence is of the form $\ell^2/(eR) = g(\ell/R)$, where the function g is expressed in terms of elliptic integrals; see Supplemental Material [23]. As a result of this analysis, we obtain the aspect ratio of the width to the height of the loop, $a = W/H$, as a function of n^2h/e. In Fig. 3, we juxtapose this result (dashed line) on top of our experimental data for all knots ($1 \le n \le 10$) and find good agreement. The slight offset of 16% may be attributed to the fact that in the experimental knots, the boundary condition at the exit point from the braid into the loop is not exactly $\theta(0) = \pi$ [23] when ϵ is small but nonzero.

Compiling the various results obtained above—namely, $R = h/\epsilon^2$, $\ell = 2n\pi/k$, $\ell^2 = eRg(\ell/R)$, as well as the relation between k and F through Eqs. (3) and (4)—we arrive at a complete solution for our knot problem:

$$n^2\frac{h}{e} = \frac{1}{8\sqrt{3}\pi^2} g\left(\left[\frac{96\sqrt{3}\pi^2}{\mu}\cdot\frac{n^2Fh^2}{B}\right]^{1/3}\right). \tag{5}$$

This expression captures the equilibrium of the loop through the known nonlinear function g, and offers a self-contained (albeit implicit) prediction for the force F as a function of the end-to-end shortening e, which is the control parameter. In Fig. 4, we compare this prediction to our experimental results for knots with $1 \le n \le 10$, using the value $\mu = 0.119$ determined earlier. We find that all the data collapse onto the master curve predicted by Eq. (5) (dashed line) [23]. It is important to highlight that, even though the analysis assumed $n \gg 1$, the agreement is excellent for $n \ge 2$ (and reasonable for $n = 1$).

This is the first time, to the best of our knowledge, that precision model experiments and theory have been tied together to untangle the influence of topology on the mechanics of knots. Our predictive framework provides concrete design guidelines for the choice of specific knot topologies depending on targeted load bearing capacities. This work could potentially be extended to obtain stress-strain relations in the braid to provide failure criteria. Beyond overhand knots, we believe that the formalism we have developed may be built upon to study the mechanics of more complex knot topologies and bundles, where frictional interactions play a major role.

We are grateful for financial support from the National Science Foundation (CMMI-1129894).

*audoly@lmm.jussieu.fr
†preis@mit.edu

[1] B. Polster, Nature (London) **420**, 476 (2002).
[2] Y. Arai, R. Yasuda, K.-i. Akashi, Y. Harada, H. Miyata, K. Kinosita, and H. Itoh, Nature (London) **399**, 446 (1999).
[3] J. C. Turner and P. van De Griend, *History and Science of Knots* (World Scientific, Singapore, 1996).
[4] D. M. Raymer and D. E. Smith, Proc. Natl. Acad. Sci. U.S.A. **104**, 16432 (2007).
[5] D. Meluzzi, D. E. Smith, and G. Arya, Annu. Rev. Biophys. **39**, 349 (2010).
[6] C. A. Zimmer, J. G. Thacker, D. M. Powell, K. T. Bellian, D. G. Becker, G. T. Rodeheaver, and R. F. Edlich, Am. J. Emerg. Med. **9**, 107 (1991).
[7] S.-H. Kim, K.-I. Ha, S.-H. Kim, and J.-S. Kim, Arthroscopy: official publication of the Arthroscopy Association of North America and the International Arthroscopy Association **17**, 850 (2001).
[8] S. Barnes, *Anglers' Knots in Gut and Nylon, Revised and Enlarged* (Cornish Bros., Birmingham, England, 1951).
[9] C. L. Day, *The Art of Knotting and Splicing* (Naval Inst. Press, Annapolis, MD, 1986).
[10] C. Wright and J. Magowan, Alpine J. **40**, 340 (1928).
[11] N. M. Pugno, PLoS One **9**, e93079 (2014).
[12] C. Adams, *The Knot Book: An Elementary Introduction to the Mathematical Theory of Knots* (AMS Bookstore, Providence, RI, 2004).
[13] C. A. Zimmer, J. G. Thacker, D. M. Powell, K. T. Bellian, D. G. Becker, G. T. Rodeheaver, and R. F. Edlich, Am. J. Emerg. Med. **9**, 107 (1991).
[14] C. Wright and J. Magowan, Alpine J. **40**, 120 (1928).
[15] M. Bergou, M. Wardetzky, S. Robinson, B. Audoly, and E. Grinspun, ACM Trans. Graph. **27**, 63 (2008);
[16] A. Konyukhov and K. Schweizerhof, in *ECCM: Solids, Structures and Coupled Problems in Engineering* (ECCM, Lisbon, 2010), pp. 324.
[17] J. H. Maddocks and J. B. Keller, SIAM J. Appl. Math. **47**, 1185 (1987).
[18] O. Gonzalez and J. H. Maddocks, Proc. Natl. Acad. Sci. U.S.A. **96**, 4769 (1999).
[19] J. P. Den Hartog, *Mechanics* (Courier Dover, New York, 2013).
[20] D. Durville, Comput. Mech. **49**, 687 (2012).
[21] B. Audoly, N. Clauvelin, and S. Neukirch, Phys. Rev. Lett. **99**, 164301 (2007).
[22] N. Clauvelin, B. Audoly, and S. Neukirch, J. Mech. Phys. Solids **57**, 1623 (2009).
[23] See Supplemental Material at http://link.aps.org/supplemental/10.1103/PhysRevLett.115.118302 for experimental details, a summary of the scaling assumptions, the numerical calculation of the nonlinear Elastica problem for the loop, photographs of knots on a Nitinol rod at high values of n, verification of the planarity of the loop, and further validation of the theory.